Enhanced tunneling conductivity induced by gelation of attractive colloids

Biagio Nigro, Claudio Grimaldi, Peter Ryser, Francesco Varrato, Giuseppe Foffi, and Peter J. Lu (□□□)

Phys. Rev. E **87**, 062312 — Published 19 June 2013

DOI: 10.1103/PhysRevE.87.062312

Enhanced tunneling conductivity induced by gelation of attractive colloids

Biagio Nigro, Claudio Grimaldi,* and Peter Ryser
LPM, Ecole Polytechnique Fédérale de Lausanne (EPFL), CH-1015 Lausanne, Switzerland

Francesco Varrato
Institute of Theoretical Physics, Ecole Polytechnique Fédérale de Lausanne (EPFL), CH-1015 Lausanne, Switzerland

Giuseppe Foffi
Institute of Theoretical Physics, Ecole Polytechnique Fédérale de Lausanne (EPFL), CH-1015 Lausanne, Switzerland and Laboratoire de Physique de Solides, UMR 8502, Bat. 510, Universite Paris-Sud, F-91405 Orsay, France

Peter J. Lu (陸述義)
Department of Physics and SEAS, Harvard University, Cambridge, Massachusetts 02138, USA

We show that the formation of a gel by conducting colloidal particles leads to a dramatic enhancement in bulk conductivity, due to inter-particle electron tunneling, combining predictions from molecular dynamics simulations with structural measurements in an experimental colloid system. Our results show how colloidal gelation can be used as a general route to huge enhancements of conductivity, and suggest a feasible way for developing cheap materials with novel properties and low metal content.

PACS numbers: 64.60.ah, 82.70.Dd, 82.70.Gg, 73.40.Gk

I. INTRODUCTION

Attractive forces between colloidal particles, ranging in size from nanometers to microns, can be finely controlled in the laboratory through surface functionalization or addition of depletants, leading to a wide range of phases and dynamical behaviors [1–5]. In particular, when the inter-particle attraction range λ is much smaller than the particle diameter D, the dynamical arrest of phase separation leads to the formation of colloidal gels—arrested, space-spanning structures—even at low particle volume fractions ϕ [6, 7]. Gels form when particles are quenched into the liquid-gas phase-separation region of the phase diagram, and spinodal decomposition arrests [7–9]; they have been observed experimentally in colloids and proteins [7, 9–13], and in computer simulations[8, 14–16]. The structure of these gels depend on ϕ, λ and the strength of the attraction [10], and can form sparse, ramified semi-solid structures.

For dispersions of conducting particles, tuning the inter-particle attractions can alter the bulk electrical properties of the system [17, 18], for example enhancing electrical conductivity in colloidal fluids [19] by lowering the mean distance required for electrons to tunnel between particles [20]. If this enhanced tunneling were to persist or be amplified in the deeply-quenched region as well, this might provide a new route to designing materials with novel combinations of electrical and mechanical properties, such as new highly-conductive semi-solid materials which could have important practical applications in energy storage and transport.

In this Article, we explore how the gelation of conducting colloidal particles affects overall electrical conductivity, where electron tunneling between particles is the principal mechanism of electrical conductivity. We find using molecular dynamics computer simulations that the tunneling conductivity σ in the arrested gel phase depends only weakly on ϕ, and remains relatively high even for ϕ as low as 3%. In this regime, we also find that σ is only moderately affected by varying ξ/D by as much as one order of magnitude, where ξ is the characteristic tunneling decay length. In addition, we perform the same analysis for gel structures formed in an experimental colloidal system with short-ranged, attractive depletion interactions; we find a similar shortening of the relevant tunneling distances as the system evolves towards the arrested gel state. Our results demonstrate that conduction via tunneling in gels of conducting colloidal particles can occur using realistic assumptions of microscopic parameters, opening up the possibility of creating new, lightweight, highly conductive materials with novel mechanical and electrical properties.

II. MODEL AND SIMULATIONS

Our simulations comprise a colloidal system of N conducting monodisperse spherical particles dispersed in an continuous insulating medium, with volume fraction $\phi = \pi\rho D^3/6$, where D is the sphere diameter, $\rho = N/L^3$ is the number density and L is the box size. We assume that the conductance between any two particles i and j is dominated by electron tunneling processes, with conductance $g(\delta_{ij})$:

$$g(\delta_{ij}) = g_0 \exp\left(-\frac{2\delta_{ij}}{\xi}\right) \tag{1}$$

where $\delta_{ij} \equiv r_{ij} - D$ is the closest distance between particle surfaces, r_{ij} is the center-to-center distance between particles, ξ is the tunneling decay length, and g_0 is a prefactor that we

* claudio.grimaldi@epfl.ch; Present address: Laboratory of Physics of Complex Matter, Ecole Polytechnique Fédérale de Lausanne (EPFL), CH-1015 Lausanne, Switzerland

define so that the conductance between two touching colloids is $g(0) \equiv 1$. The potential barrier separating conducting and insulating phases determines ξ, which typically ranges from a fraction of a nanometer to a few nanometers [21]. Consequently, $\xi/D \lesssim 0.1$ for particles larger than a few tens of nanometers, so that, consistently with Eq. (1), charging and Coulomb interaction effects on electron transfer can be safely neglected at room temperature.

For colloidal systems with short-ranged attractions, $\lambda/D \lesssim 0.05$, thermodynamic properties at a given ϕ depend not on the specific shape of the potential $u(r)$, but only on its integral, expressed as a reduced second virial coefficient $B_2^* = (3/D^3)\int[1-e^{-u(r)/T}]r^2dr$, where T is the temperature and $k_B \equiv 1$ [7, 22–24]. In particular, short-ranged attractive colloidal spheres are in an equilibrium fluid phase for $B_2^* \gtrsim B_2^{*c}$, where $B_2^{*c} \simeq -1.2$ is the critical value at the critical point of the gas-liquid phase separation [25, 26]. Because all short-range potential shapes yield the same thermodynamic behavior [7, 22], we select a square-well (SW) model of the interaction of the form:

$$u(\delta_{ij}) = \begin{cases} \infty & \delta_{ij} \leq 0 \\ -u_0 & 0 < \delta_{ij} \leq \lambda D \\ 0 & \delta_{ij} > \lambda D \end{cases} \qquad (2)$$

where $\lambda \ll 1$ and $u_0 > 0$ are, respectively, the dimensionless potential range and depth. As in Eq. (1), δ_{ij} denotes the closest distance between surfaces of particle pairs. The scaled virial coefficient of the potential in Eq. (2) can be expressed as $B_2^* \equiv 1 - 1/4\tau$, where $\tau^{-1} \equiv 4[(1+\lambda)^3-1][\exp(u_0/T)-1]$ is the Baxter stickiness parameter [28]. Consequently, a homogeneous SW fluid exists when τ is greater than the critical value $\tau_c \sim 0.11$ [25, 26].

In this regime, SW fluids of conducting particles display enhanced conductivity σ, relative to the hard-sphere case, as τ is decreased [20]. The inter-particle attraction enhances conductivity by drawing the particles closer together: the population of particles with separations lower than λD increases, thereby promoting short-length tunneling processes, which result in larger $g(\delta_{ij})$. Specifically, in attractive colloidal fluids where $\lambda \to 0$, $\tau = 0.2$, and $\xi/D = 0.01$, σ is relatively large and depends only weakly on ϕ for $\phi \gtrsim 0.2$.[20]

When $B_2^* \leq B_2^{*c}$ (i.e., $\tau \leq \tau_c$), short-ranged attractive colloids undergo phase separation and can arrest to form gels: spanning structures that may sustain shear stresses even at low ϕ [7, 8, 15, 16]. In these gel configurations, larger tunneling conductivities might be expected relative to the fluid phase at the same ϕ, as the mean separation between the particles forming the gel network falls below λD; however, knowledge of potential range alone is insufficient to predict the conductivity level of the system, as previously shown for SW fluids of conducting colloids [20]. Instead, the full interplay between tunneling, attraction and structure must be considered.

III. MOLECULAR DYNAMICS SIMULATIONS

We generate colloidal gel structures from molecular dynamics (MD) simulations of $N = 10^4$ attractive colloids of mass m, square well depth $u_0 = 1$, and $\lambda = 0.03$, corresponding to a critical temperature $T_c \simeq 0.3$. We implement Newtonian dynamics via a standard event-driven algorithm [15, 29]. At $t = 0$ we equilibrate initial configurations at $T = 100 \gg T_c$, where these systems behave as hard-sphere (HS) fluids: $B_2^* \sim 1$. For each selected ϕ value we consider 30 independent realizations. We define two particles as bonded when $\delta_{ij} \leq \lambda D$, so that the average number of bonds per particle is $n_b = -2U/(Nu_0)$, where U/N is the potential energy per particle. For $t > 0$, we quench the system to $T_q = 0.05 \ll T_c$, corresponding to $\tau \simeq 5.56 \times 10^{-9}$ and $B_2^* \simeq -4.5 \times 10^7$; we select five different packing fractions, ranging from $\phi \simeq 0.03$ to $\phi \simeq 0.3$, marked with circles in Fig. 1(a). These configurations fall well within the two-phase region of the phase diagram; the full gas-liquid coexistence line at this attraction range [25–27] is marked with squares in

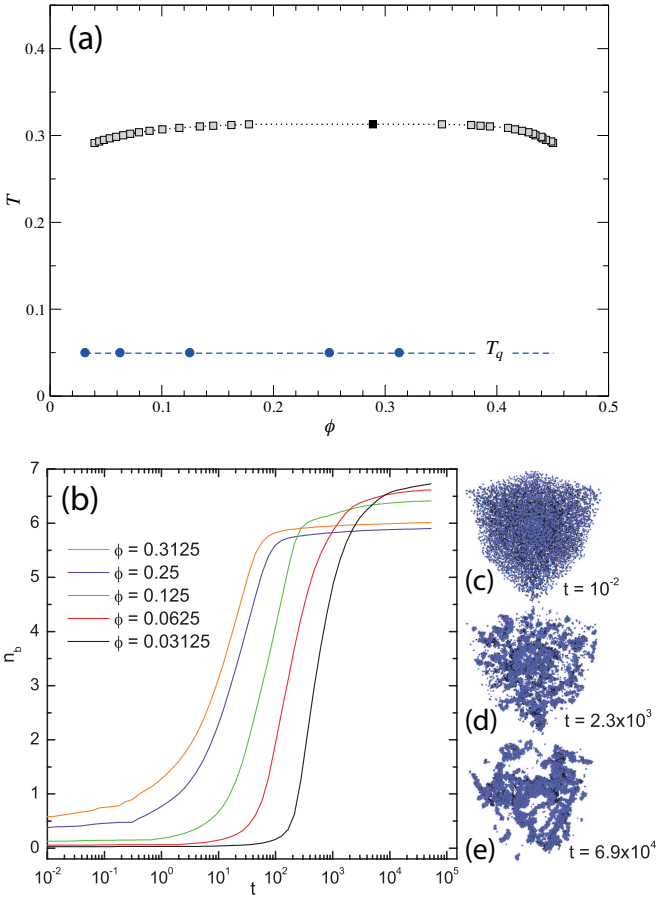

FIG. 1. (Color online) (a) Phase diagram for the $\lambda = 0.03$ SW system. The binodal and the critical point are represented by open and closed squares, respectively. The gel points, obtained by quenching to state points at low temperature T_q, are represented by circles. (b) Average number of bonds n_b for different ϕ as a function of t, expressed in units of $D\sqrt{m/u_0}$. Three different stages of aggregation for $\phi = 0.03125$ are shown for (c) $t = 0.01$, (d) $t = 2.3 \times 10^3$, and (e) $t = 6.9 \times 10^4$. The configuration shown in (e) represents an arrested colloidal gel, where the particle positions do not display any subsequent time evolution.

the figure.

At short times, the samples appear homogeneously dispersed, as illustrated by a sample with $\phi = 0.03125$ in Fig. 1(c); this fluid-like initial state, where $n_{\rm b}$ remains at a constant low level, persists longer for lower ϕ, as shown in Fig. 1(b). Following this initial transient state, concentration fluctuations arising from spinodal decomposition grow rapidly, marked by a steep rise in $n_{\rm b}$, as illustrated in Fig. 1(d). Eventually, when the particles become so dense locally as to potentially undergo an attractive glass transition [7], the structures arrest to form gels, as illustrated in Fig. 1(e), and $n_{\rm b}$ plateaus at about 6; no further evolution is observed.

IV. CRITICAL PATH APPROXIMATION

To explore the effect of gelation on the system conductivity σ we first apply the critical path approximation (CPA) to the network formed by the tunneling conductances of Eq. (1) [30]. When the δ_{ij} distances are widely distributed on a length scale of the order of ξ, the CPA provides a robust estimate of the network conductivity through

$$\sigma_{\rm cpa} = \sigma_0 \exp\left(-\frac{2\delta_c}{\xi}\right), \qquad (3)$$

where σ_0 is a constant prefactor and δ_c is the shortest δ_{ij} such that the subnetwork defined by the bonds satisfying $\delta_{ij} \leq \delta_c$ forms a percolating cluster [20, 31]. Equation (3) thus replaces the problem of solving the tunneling network equations by a simpler one: finding the critical distance δ_c so that percolation is established. Depending on the particle concentration and the potential depth, δ_c may be larger or lower than the attraction range λD [20].

To calculate δ_c, we coat each conducting sphere with a concentric penetrable shell of thickness $\delta_0/2$, for each configuration of the system at a given volume fraction ϕ and time t; we consider two spheres as connected if their penetrable shells overlap (*i.e.*, if $\delta_{ij} \leq \delta_0$). Using a clustering algorithm [32], we compute the minimum value δ of δ_0 such that a cluster of connected particles connects two opposite faces of the simulation box. We repeat this procedure along all three axes of the cubic box, so that a total of 90 values of δ are calculated for each ϕ and t. By counting the number of instances for which sample-spanning clusters appear for a given δ, we construct the percolation probability $P(\delta)$, shown in Figs. 2(a)-2(c) for systems with $\phi = 0.03125, 0.125$ and 0.3125, respectively. In each panel of Figs. 2(a)-2(c) we plot $P(\delta)$ for several values of t, expressed in units of $D\sqrt{m/u_0}$, ranging from the onset of the quench at $t = 0.013$, to the longest time $t = 6.86 \times 10^4$, when the gel phase is fully formed for all ϕ.

Gelation considerably lowers the values of δ for which $P(\delta)$ increases from 0 to 1, as shown in Fig. 2(a), indicating that gel networks percolate at smaller distances than that of the fluid state at the same ϕ. In addition, we observe a sudden change in the slope of $P(\delta)$ when δ/D crosses λ, marked with vertical dashed lines, due to the discontinuity of the SW potential, as seen for $\phi = 0.3125$ and 0.03125 and already observed in SW fluids [20]. Furthermore, for $\phi = 0.03125$ the percolation transition is not monotonic and, at large times, $P(\delta)$ reaches the unity only for very large δ; in these cases, the finite size of the system prevents some realizations of the gel network with $\phi = 0.03125$ from connecting two opposite faces of the box. We minimize finite-size effects by choosing suitable criteria for extracting δ_c from $P(\delta)$; using the criterion $P(\delta_c) = 1/2$ to define the critical distance, we find estimates of δ_c from $N = 10^4$ particles to differ from the $N \to \infty$ limit by only a few percent, as shown in the appendix.

To understand the dynamics of these systems, we investigate the time evolution of δ_c for all ϕ. At short times, particles are dispersed nearly homogeneously, so that δ_{ij}, and thus δ_c, decrease strongly as ϕ increases, as shown in Fig. 3(a) and in agreement with previous results on SW equilibrium fluids [20]. However, when the system is arrested at long times, the vast majority of particles forming the spanning gel structure have separations lower than λD, consistent with the data shown in Fig. 1(b), where the number of bonds stabilizes at $n_b \approx 6$ for large t. Consequently, δ_c becomes small, about $0.01D$, and independent of ϕ, as shown in Fig. 3(a). Strikingly, though the final value of δ_c is the same for all ϕ, we observe significant ϕ-dependent differences in reaching this state: for the three largest concentrations, δ_c monotonically approaches the arrested state value, as shown by dashed lines in Fig. 3(a); by contrast, for $\phi = 0.0613$ and 0.03125, δ_c exhibits a pronounced maximum at intermediate times, followed by a sudden drop towards the arrested state, shown with solid lines in the figure, which may reflect the formation and subsequent disappearance of a fluid of particle clusters [10]. In this intermediate regime, where the particles are largely aggregated into nearly close-packed clusters, illustrated in Fig. 1(d), the mean distance between clusters is larger at lower ϕ. Therefore, percolation occurs only for higher δ_c, as shown in Fig. 3(a).

To assess the applicability of these simulation predictions to physical systems, we repeat analysis on gels formed in an experimental attractive colloid system [7]. We use sterically-stabilized polymethylmethacrylate (PMMA) spheres in a solvent mixture of decahydronaphtalene and bromocyclohexane [10], with $D \simeq 1120$ nm and $\phi = 0.045$, and introduce a non-adsorbing linear polymer, polystyrene with molecular weight $M_{\rm W} = 695,000$, that forms random coils in solution with radius $R_p = 33$ nm, so that $\lambda = 0.06$ [7]. We select a sample with polymer concentration $c_{\rm p}$=3.31 mg/ml, which phase separates and arrests to form a gel [7]. Using confocal microscopy [33], we locate each particle individually [7, 10, 33], thereby allowing the same analysis as performed on the MD simulation configurations. We observe that the evolution of experimental δ_c is in qualitative agreement with the MD simulations at similar ϕ, as shown in Fig. 3(b). Although the initial low-time plateau cannot be sampled practically in these experiments, a maximum of δ_c is discernible at $t \approx 300$ s, followed by a rapid drop of δ_c at longer times. For $t \gtrsim 10^4$ s, the system reaches the arrested gel state, and $\delta_c/D \approx 0.1$, independent of time. This transition associated with the formation of an arrested gel, consistent with behavior observed in simulations, is illustrated by the renderings of the

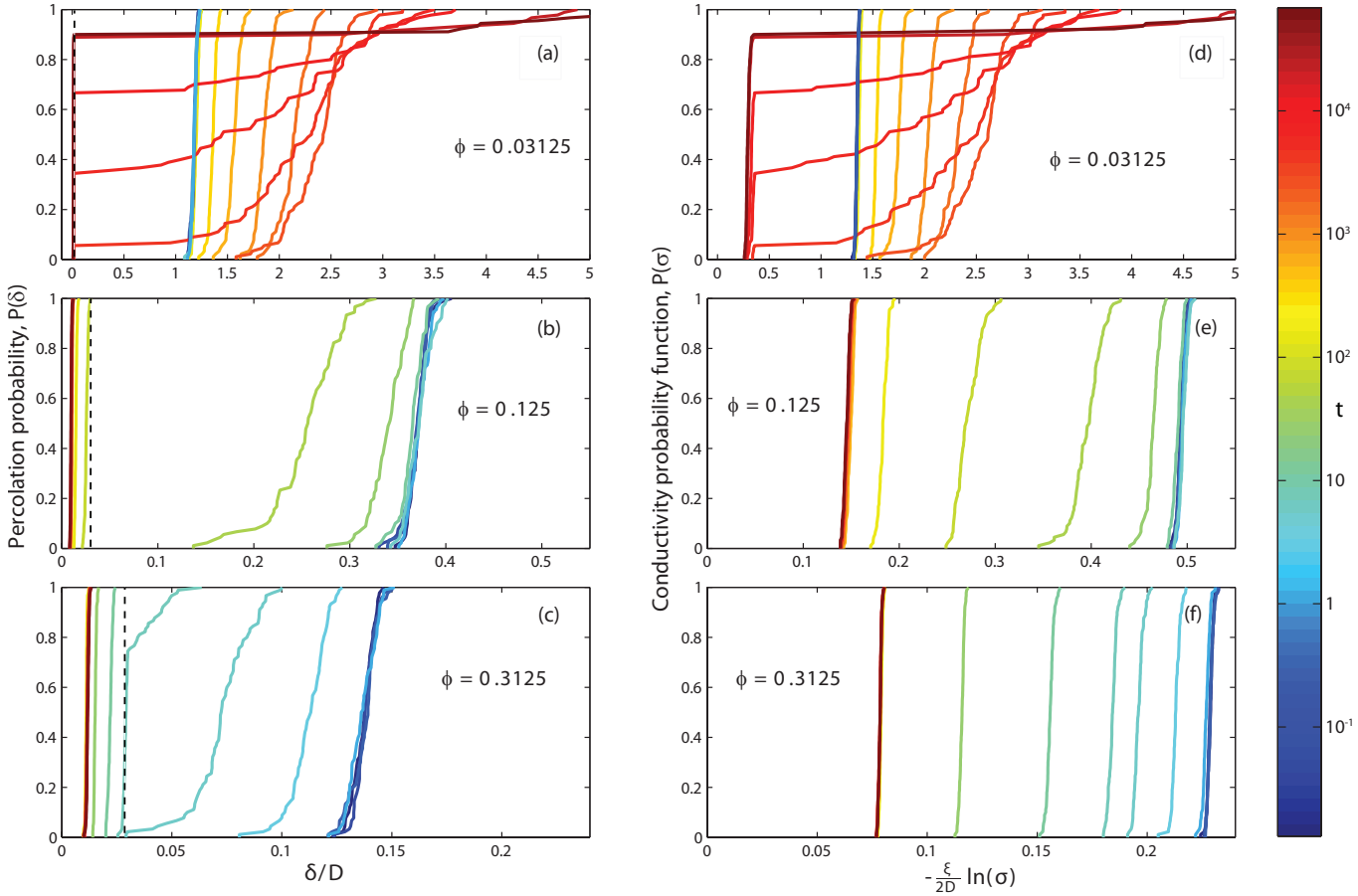

FIG. 2. (Color online) Time evolution of percolation probability $P(\delta)$ for the connectivity distance δ/D for (a) $\phi = 0.03125$, (b) $\phi = 0.125$, and (c) $\phi = 0.3125$. The vertical dashed line in (a)-(c) indicates $\delta/D = \lambda = 0.03$. For each ϕ, each curve represents $P(\delta)$ calculated at a specific time ranging from $t = 0.013$ to $t = 6.86 \times 10^4$, illustrated with the color (gray) bar at right. (d)-(f): conductivity probability $P(\sigma)$ as function of $-\frac{\xi}{2D}\ln(\sigma)$ for tunneling decay length fixed at $\xi/D = 0.1$.

measured particle positions in Fig. 3(b).

We combine the time evolution predictions for δ_c, as shown in Fig. 3(a), with Eq. (3), to yield an estimate for the time evolution of $\sigma_{\rm cpa}$, and observe that a broad distribution of ϕ-dependent $\sigma_{\rm cpa}$ conductivities, spanning about ten orders of magnitude, drastically narrows in the arrested gel state, where $\sigma_{\rm cpa}$ remains at a constant high value for all ϕ [34], as shown for $\xi = 0.1D$ with solid lines in Fig. 4. Interestingly, for the two lowest ϕ values, the maximum of δ_c due to the transitory fluid of clusters is reflected by a huge minimum of $\sigma_{\rm cpa}$; fluids of clusters of conducting particles appear to be substantially worse conductors than a homogeneous fluid of the same composition.

V. NUMERICAL CALCULATION OF THE NETWORK CONDUCTIVITY

To test the accuracy of the results obtained using the CPA, shown in Fig. 4, we solve numerically the tunneling resistor network equations: for each simulation-generated configuration, we assign the inter-particle conductances from Eq. (1) to each pair of particles, thereby generating a fully-connected network. To reduce the number of tunneling connections, we introduce a maximum tunneling distance $\delta_{\rm max}$ so that the conductances between particles at mutual distances $\delta_{ij} > \delta_{\rm max}$ are neglected; this does not affect overall conductivity [35]. For all realizations, we calculate the conductance G of the reduced network by combining numerical decimation with a preconditioned conjugate gradient method [20]. From the dimensionless conductivity $\sigma = GD/L$, where L is the simulation box edge, we construct the conductivity probability $P(\sigma)$ obtained from all configurations with fixed ϕ and t, as shown for tunneling decay length fixed at $\xi/D = 0.1$ in Figs. 2(d)-2(f).

In general, we find qualitative correspondence between $P(\sigma)$ and $P(\delta)$, which can be seen by comparing Figs. 2(a)-2(c) with Figs. 2(d)-2(f). $P(\sigma)$ and $P(\delta)$ agree even quantitatively for the $\phi = 0.03125$, and for t when the structure is not yet arrested; in this regime $\delta \gtrsim \xi$, and the CPA pro-

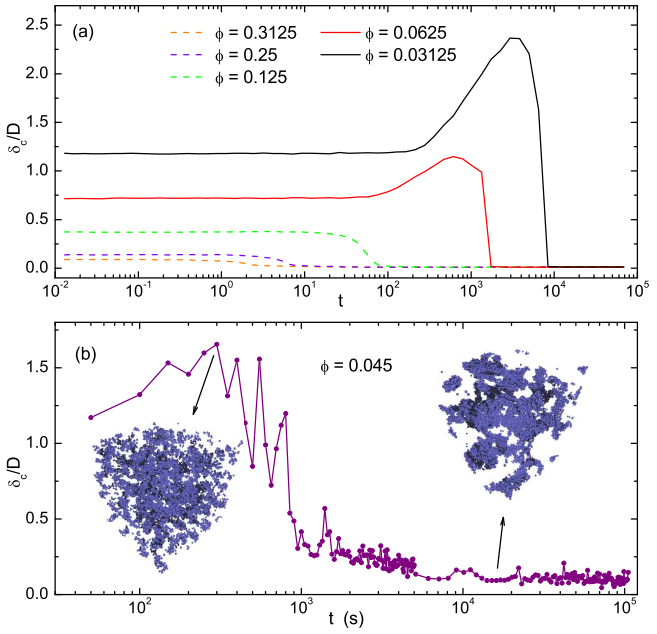

FIG. 3. (Color online) (a) Time evolution of the critical connectedness distance δ_c for gels simulated at different ϕ, with t in units of $D\sqrt{m/u_0}$. (b) Time evolution (in seconds) of the critical distance extracted from the measured spatial positions of PMMA particles in a polymer-colloid system [7]. For times larger than about 10^4 s the system is in an arrested gel state.

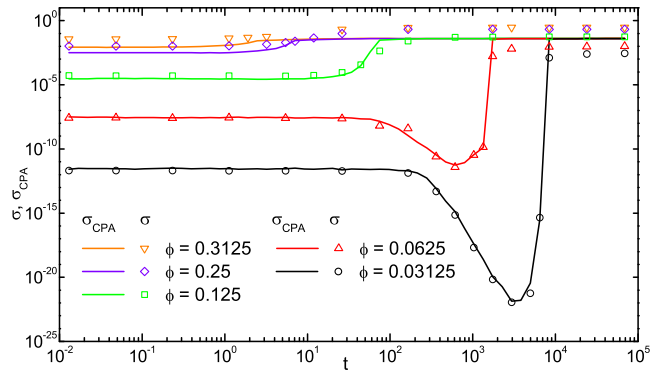

FIG. 4. (Color online) Time evolution of conductivity σ for $\xi/D = 0.1$ during the formation of the colloidal gel. Numerical solution of the tunneling resistor equations shown with symbols; $\sigma_{\rm CPA}$ obtained from Eq. 3 using $\sigma_0 = 0.1$, with solid lines.

vides a good approximation of σ. These data confirm the validity of using $P(\sigma) = 1/2$ to define the network conductivity σ, which we find valid also when $\delta \lesssim \xi$, as shown in the appendix. Beginning from the liquid-like states through the onset of gelation, the σ values obtained through this network approach closely follow the corresponding $\sigma_{\rm cpa}$ values, as shown in Fig. 4 with symbols and lines, respectively. Slight discrepancies in the ϕ-dispersion of arrested states likely arise from the short- and moderately-dispersed distances between

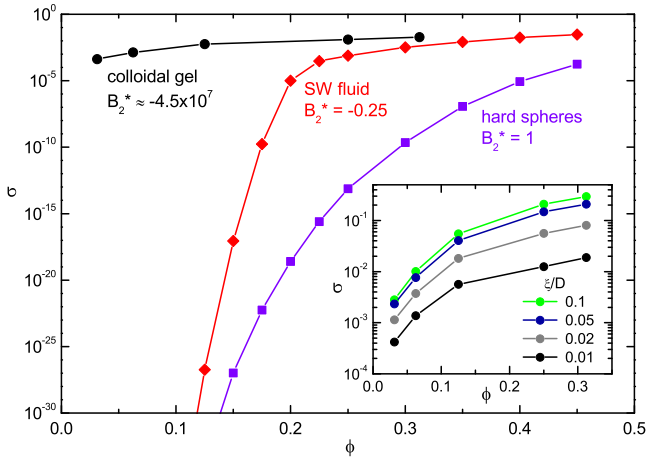

FIG. 5. (Color online) Conductivity σ as a function of ϕ for the arrested gel state (filled circles), equilibrium SW fluids (filled diamonds), and equilibrium HS fluids (squares). In all cases, $\xi/D = 0.01$. Inset: ϕ-dependence of σ for the arrested gel state calculated for different values of ξ/D.

the neighboring particles of the spanning gel structure, which make Eq. (3) less accurate, as previously discussed.

The significantly higher σ in the long-time arrested gel state relative to the initial fluid-like state, most pronounced for low ϕ and highlighted in Fig. 4, suggests the general possibility that arrested gel structures could have higher σ relative to other structures formed from tunneling particles in colloidal suspensions at the same ϕ. To test this possibility, we use Monte-Carlo simulations to generate equilibrium fluids of both HS and SW particles at various ϕ, with $\lambda = 0.03$ and $\tau = 0.2 > \tau_c$. For each ϕ, we obtain 300 independent equilibrium configurations of systems with $N = 2000$ particles; we determine σ for $\xi/D = 0.01$ and compare with the long-time σ of the arrested gel state as a function of ϕ. In all cases, at any given ϕ, the gel state has a higher σ than that of the SW fluid, which in turn is always higher than that of the hard-sphere fluid, as shown in Fig. 5 with circles, diamonds and squares, respectively. The σ values for gel and SW fluid converge for high $\phi \gg 0.3$; by contrast, for $\phi \lesssim 0.2$, σ of the arrested state is many orders of magnitude higher than that of either fluid. Interestingly, while σ depends heavily on ϕ in both fluid cases, it is relatively constant in the gel case, even for $\phi \simeq 0.03$, as shown in Fig. 5.

Finally, to explore how the conductivity varies with tunneling decay length, we calculate σ of arrested gels with different ϕ and ξ/D. We observe that σ only weakly depends on ξ/D in the gel state, due to short inter-particle distances within the gel, as shown in the inset to Fig. 5. Indeed, the relevant length-scale is δ_c/D; in the arrested state we find $\delta_c \simeq 0.01D$ and tunneling is thus generally unaffected so long as $2\delta_c/\xi \lesssim 1$, that is, as long as $\xi/D \gtrsim 0.02$. At much lower values, ξ/D suppresses inter-particle tunneling, so that σ is small even in the arrested gel state.

VI. DISCUSSION AND CONCLUSIONS

Our data and analyses suggest that, in the arrested regime—where the colloidal conducting particles form system-spanning amorphous gel structures—the conductivity can be large and only weakly depends on ϕ. These results may impact real-world colloidal systems, where the solid properties of colloidal gels can be combined with high electrical conductivities to develop materials with novel mechanical and electrical properties. In contrast to other systems where conducting particles are embedded in pre-existing gel networks [36], in our conducting colloidal gels the conducting particles create simultaneously both the gel network and the conducting path. This synergy can be exploited, at least in principle, to control the conductivity directly through the attraction between the particles, or to change the gel structure by local heating of the tunneling-gel network.

Our simulation results demonstrate that conduction by tunneling can be strongly enhanced by the formation of arrested colloidal gel structures; however, the precise experimental conditions under which systems of real conducting colloidal systems show similar performance is not yet known. In general, polymers mediating depletion attractions have gyration radii larger than about 1-5 nm [37]; therefore, requiring ξ/D to be no more than a few percent requires $D \gtrsim 50$ nm. Encouragingly, with particles of this size and typical tunneling decay lengths of a few nm, conductivities like those in Fig. 5 may yet be achievable in the lab. Nevertheless, conducting particles in this size range remain a significant synthetic challenge, and suspensions of larger metallic particles show significant sedimentation that may compromise the formation of gels. Potential solutions to this problem include using metal-coated PMMA particles, low-structured carbon black particles, conducting polymer particles, or synthesizing gels in a micro-gravity environment, such as that provided by the International Space Station.

ACKNOWLEDGMENTS

B. N. acknowledges financial support by the Swiss National Science Foundation (grant No. 200020-135491). F. V. and G. F. acknowledge financial support by the Swiss National Science Foundation (grants No. PP0022-119006 and PP00P2-140822/1). P. J. L. performed the experimental work in the laboratory of Prof. D. A. Weitz at Harvard University, and acknowledges financial support from NASA (NNX08AE09G, NNX08AE09G S11, NNC08BA08B), the NSF (DMR-1006546), the Harvard MRSEC (DMR-0820484).

Appendix A: Finite-size analysis of δ_c and σ

We present finite-size scaling analyses of the percolation probability $P(\delta)$ and of the conductivity probability $P(\sigma)$, demonstrating the validity of the criteria $P(\delta_c) = 1/2$ and $P(\sigma) = 1/2$ to define the critical distance δ_c and the network conductivity σ.

TABLE I. Finite-size scaling results for δ_c at $N \to \infty$ extracted from the fits shown in Fig. 7 and the corresponding values obtained by using $P(\delta_c) = 1/2$ for $N = 10^4$.

time	$\delta_c(N \to \infty)$	$\delta_c(N = 10^4)$
$t_1 = 0.01$	0.3709 ± 0.0007	0.3711
$t_2 = 39.9$	0.2235 ± 0.0076	0.2270
$t_3 = 53.1$	0.100 ± 0.006	0.1062
$t_4 = 70.7$	0.0264 ± 0.0003	0.0265
$t_5 = 475.7$	0.0106 ± 0.0001	0.0108

TABLE II. Finite-size scaling results for σ at $N \to \infty$, extracted from the fixed points of $P(\sigma)$ of Fig. 5 and the corresponding values obtained by using $P(\sigma) = 1/2$ for $N = 10^4$.

time	$-\frac{\xi}{2D} \ln \sigma(N \to \infty)$	$-\frac{\xi}{2D} \ln \sigma(N = 10^4)$
$t_1 = 0.01$	0.4991 ± 0.0006	0.4933
$t_2 = 39.9$	0.3957 ± 0.0014	0.3809
$t_3 = 53.1$	0.3485 ± 0.0021	0.3314
$t_4 = 70.7$	0.2957 ± 0.0017	0.2854
$t_5 = 475.7$	0.1508 ± 0.0003	0.1503

1. Critical distance δ_c

To demonstrate the finite-size method to determine δ_c we construct the percolation probability $P(\delta)$, as described in Sec. IV, for particle volume fraction fixed at $\phi = 0.125$ and for different times t and particle number N, as shown in Figs. 6(a), with corresponding fits to $P(\delta)$ obtained from linear combinations of two error functions in and Fig. 6(b). For the cases with $N > 5000$, the fixed point of the percolation probability—the point at which the $P(\delta)$ curves for different N intersect each other—is located approximately at $P = 1/2$, which we use to define critical distance δ_c. To test how this might change with system size, we apply to each $P(\delta)$ the finite-size scaling relation:

$$\delta_c - \delta_c(N) \propto N^{-1/3\nu}, \tag{A1}$$

where $\nu \simeq 0.88$ is the correlation length exponent and $\delta_c(N)$ is the value of the critical distance extracted from the fitted curves at exactly $P(\delta_c(N)) = 1/2$. From the evolution of $\delta_c(N)$ as a function of $N^{-1/3\nu}$, we extract δ_c for $N \to \infty$ from the intercept at $N^{-1/3\nu} = 0$, shown in Fig. 7. By comparing these δ_c values with those extracted from the condition $P = 1/2$ applied to the $N = 10^4$ cases, we find that at worst, $\delta_c(N = 10^4)$ is only 6% lower than its asymptotic estimate at $N \to \infty$, as seen in Table I.

2. Conductivity

To demonstrate that $P(\sigma) = 1/2$ is a valid criterion to extract the network conductivity σ, we calculate $P(\sigma)$ for $\xi/D = 0.1$, $\phi = 0.125$, and various N and t values, shown

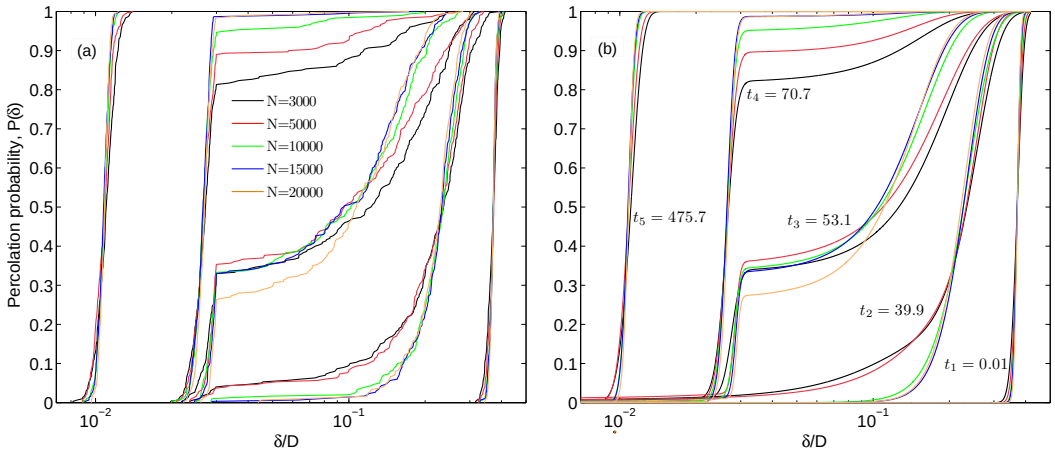

FIG. 6. (Color online) (a) Percolation probability $P(\delta)$ as a function of the connectivity distance δ at $\phi = 0.125$ for different time t (in units of $D\sqrt{m/u_0}$) and particle numbers N. (b) Fits to the results of (a) using a combination of two error functions.

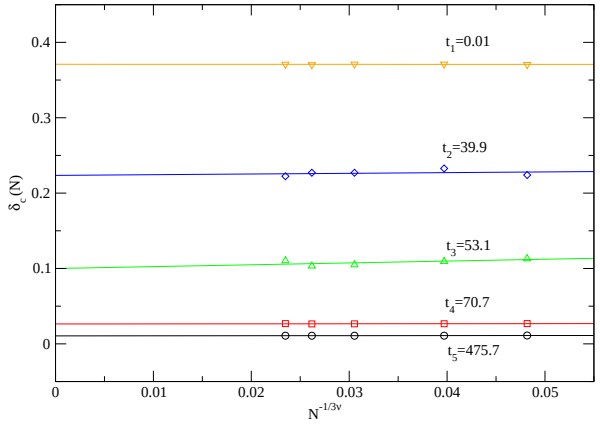

FIG. 7. (Color online) Finite-size scaling analysis of the $\delta_c(N)$ values extracted from $P(\delta_c(N)) = 1/2$ of Fig. 3. Solid lines are fits to Eq. (A1).

in Fig. 8. We find that the curves of $P(\sigma)$ do not follow the behavior of the corresponding curves of $P(\delta)$, as seen by comparing Fig. 8 with Fig. 6, where $P(\delta)$ is plotted for the same N and t values. In particular, $P(\sigma)$ is not affected by the discontinuity of the SW potential, in contrast to the behavior of $P(\delta)$ when $\delta/D = \lambda$. Furthermore, the fixed points detected at the crossing of the $P(\sigma)$ as N varies are no longer associated to $P = 1/2$ for N large. However, since the locations of the fixed points of $P(\sigma)$ are much more precise than those for $P(\delta)$, they can be used to extract the network conductivity $\sigma(N \to \infty)$ with great accuracy. We compare the so-obtained $\sigma(N \to \infty)$ values with those obtained from the condition $P = 1/2$ applied to systems with number of particles fixed at $N = 10^4$ in Table II; we see that the $P = 1/2$ criterion applied to the cases with $N = 10^4$ determines σ within $\sim 5\%$ of the network conductivity for $N \to \infty$.

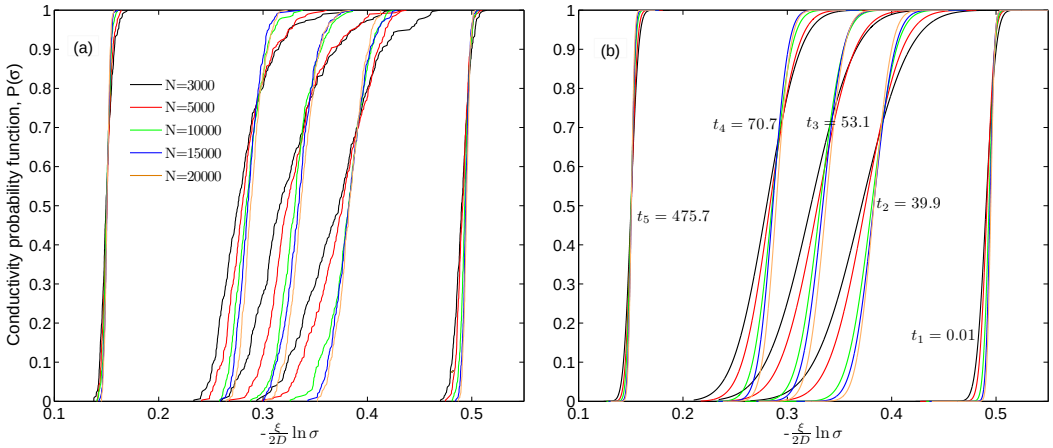

FIG. 8. (Color online) (a) Conductivity probability $P(\sigma)$ as a function of $-\frac{\xi}{2D}\ln(\sigma)$ at $\phi = 0.125$ for different values of t (in units of $D\sqrt{m/u_0}$) and particle numbers N. The tunneling decay length is $\xi = 0.1D$. (b) Fits to the results of (a) using a combination of two error functions.

[1] W. C. K. Poon, Curr. Opin. Colloid Interface Sci. **3**, 593 (1998).
[2] V. J. Anderson and H. N. W. Lekkerkerker, Nature **416**, 811 (2002)
[3] F. Sciortino, Nat. Mater. **1**, 145 (2002)
[4] D. Frenkel, Science **314**, 768 (2006)
[5] H. N. W. Lekkerkerker and R. Tuinier, *Colloids and the Depletion Interaction* (Springer, Dordrecht, 2011).
[6] S. Manley et al., Phys. Rev. Lett. **93**, 108302 (2004).
[7] P. J. Lu, E. Zaccarelli, F. Ciulla, A. B. Schofield, F. Sciortino, and D. A. Weitz, Nature **453**, 499 (2008).
[8] G. Foffi, C. De Michele, F. Sciortino, and P. Tartaglia, Phys. Rev. Lett. **94**, 078301 (2005).
[9] E. Zaccarelli, P. J. Lu, F. Ciulla, D. A. Weitz, and F. Sciortino, J. Phys. Condens. Matter **20**, 494242 (2008).
[10] P. J. Lu, J. C. Conrad, H. M. Wyss, A. B. Schofield, and D. A. Weitz, Phys. Rev. Lett. **96**, 028306 (2006).
[11] W. C. K. Poon, J. Phys. Condens. Matter **14**, R859 (2002).
[12] L. Cipelletti and L. Ramos, J. Phys. Condens. Matter **17**, R253 (2005).
[13] F. Cardinaux, T. Gibaud, A. Stradner, and P. Schurtenberger, Phys. Rev. Lett. **99**, 118301 (2007).
[14] K. G. Soga, J. R. Melrose, and R. C. Ball, J. Chem. Phys. **108**, 6026 (1998).
[15] G. Foffi, C. De Michele, F. Sciortino and P. Tartaglia, J. Chem. Phys. **122**, 224903 (2005)
[16] E. Del Gado, J. Phys. Condens. Matter **22**, 104117 (2010).
[17] B. Vigolo, C. Coulon, M. Maugey, C. Zakri, and P. Poulin, Science **309**, 920 (2005).
[18] A. V. Kyrylyuk, M. C. Hermant, T. Schilling, B. Klumperman, C. E. Koning, and P. van der Schoot, Nat. Nanotechnol. **6**, 364 (2011).
[19] T. Schilling, S. Jungblut, and M. A. Miller, Phys. Rev. Lett. **98**, 108303 (2007).
[20] B. Nigro, C. Grimaldi, M. A. Miller, P. Ryser, and T. Schilling, J. Chem. Phys. **136**, 164903 (2012).
[21] A. V. Nabok, J. Massey, S. Buttle, and A. K. Ray, IEE Proc.-Circuits Devices Syst. **151**, 461 (2004); G. Sedghi et al., Nat. Nanotechnol. **6**, 517 (2011).
[22] M. G. Noro and D. Frenkel, J. Chem. Phys. **113**, 2941 (2000).
[23] G. Foffi and F. Sciortino, Phys. Rev. E **74**, 050401(R) (2006).
[24] A. Malijevsky, S. B. Yuste, and A. Santos, J. Chem. Phys. **125**, 074507 (2006).
[25] M. A. Miller and D. Frenkel, Phys. Rev. Lett. **90**, 135702 (2003).
[26] J. Largo, M. A. Miller, and F. Sciortino, J. Chem. Phys. **128**, 134513 (2008).
[27] M. A. Miller, and D. Frenkel, J. Chem. Phys. **121**, 535 (2004).
[28] R. J. Baxter, J. Chem. Phys. **49**, 2770 (1968).
[29] D. C. Rapaport, *The Art of Computer Simulations*, 2nd ed. (Cambridge University Press, London, 1997).
[30] V. Ambegaokar, B. I. Halperin, and J. S. Langer, Phys. Rev. B **4**, 2612 (1971); M. Pollak, J. Non-Cryst. Solids **11**, 1 (1972); B. I. Shklovskii and A. L. Efros, Sov. Phys. JETP **33**, 468 (1971); **34**, 435 (1972).
[31] G. Ambrosetti, C. Grimaldi, I. Balberg, T. Maeder, A. Danani, and P. Ryser, Phys. Rev. B **81** , 155434 (2010).
[32] B. Nigro, G. Ambrosetti, C. Grimaldi, T. Maeder, and P. Ryser, Phys. Rev. B **83**, 064203 (2011).
[33] P. J. Lu, P. A. Sims, H. Oki, J. B. Macarthur, and D. A. Weitz, Opt. Express **15** 8702 (2007).
[34] In plotting the CPA conductivity results of Fig. 4 we have fixed the prefactor appearing in Eq. 3 to $\sigma_0 = 0.1$, which is the value found for hard-spheres fluids [20].
[35] For each realization of the system we first calculate the minimum connectivity length δ for a given ϕ and t, as described in Sec. IV. We then chose $\delta_{\max}$ as to satisfy $\exp(-2\delta_{\max}/\xi) = \exp(-M)g(\delta)$, where $g(\delta) = \exp(-2\delta/\xi)$ and $M = 20$, 10, 5 for $g(\delta) < 10^{-50}$, $10^{-50} < g(\delta) < 10^{-10}$, and $10^{-10} < g(\delta)$, respectively.
[36] A. Fizazi, J. Moulton, K. Pakbaz, S. D. D. V. Rughooputh, Paul Smith, and A. J. Heeger, Phys. Rev. Lett. **64**, 2180 (1990).
[37] S. Ramakrishnan, M. Fuchs, K. S. Schweizer, and C. F. Zukoski, J. Chem. Phys. **116**, 2201 (2002); S. A. Shah, Y.-L. Chen, S. Ramakrishnan, K. S. Schweizer, and C. F. Zukoski, J. Phys. Condens. Matter **15**, 4751 (2003).